Low-Temperature Luminescence in Organic Helicenes: Singlet versus Triplet State Circularly Polarized Emission

Kais Dhbaibi, Pierpaolo Morgante, Nicolas Vanthuyne, Jochen Autschbach, Ludovic Favereau, Jeanne Crassous

Low Temperature Luminescence in Organic Helicenes: Singlet Versus Triplet State Circularly Polarized Emission

Kais Dhbaibi,[a] Pierpaolo Morgante,[b] Nicolas Vanthuyne,[c] Jochen Autschbach[b,] Ludovic Favereau,[a,*] and Jeanne Crassous[a,*]*

[a] Univ Rennes, CNRS, ISCR-UMR 6226, ScanMAT–UMS 2001, F-35000 Rennes, France. E-mails: ludovic.favereau@univ-rennes1.fr; jeanne.crassous@univ-rennes1.fr

[b] Department of Chemistry, University at Buffalo, State University of New York, Buffalo, NY 14260, USA. E-mail: jochena@buffalo.edu

[c] Aix Marseille University, CNRS Centrale Marseille, iSm2, 13284 Marseille, France.

ABSTRACT. The experimental measurement of the photophysical and chiroptical properties of helicene-based π-conjugated emitters with electron accepting (-CN, -py, -NO_2) or donating (TMS, NMe_2, NH_2) moieties is reported using a new low-temperature (77 K). The samples exhibit a strong circularly polarized phosphorescence in frozen solution of 2-MeTHF, with an anisotropy factor reaching 1.6×10^{-2} and a lifetime of over 0.46 s for the most active molecule, the nitro compound. The theoretical investigation shows that although the singlet (S_1) and triplet (T_1) excited state emissions are mainly arising from the helicene core, the rotatory strengths of the spin-allowed vs.

spin-forbidden emission have opposite signs. Further analysis of the spin-orbit coupling matrix elements shows that there is no mixing between S_1 and T_1, justifying the different sign of the rotatory strengths. In the case of the nitro compound, the enhanced phosphorescence emission is due to an efficient inter-system crossing.

TOC GRAPHIC

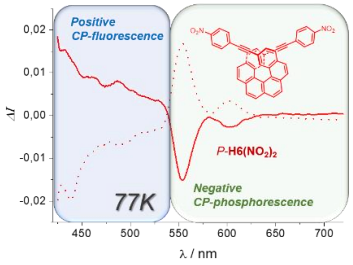

KEYWORDS. Triplet state emission, phosphorescence, spin-orbit coupling, circularly polarized emission, low temperature CPL

In the last decade, studies on circularly polarized luminescence (CPL) have seen a renewed interest due to the recent availability of commercial circularly polarized (CP) spectrofluorometers.[1-5] This technological progress has enabled the development and evaluation of the CPL of different classes of chiral emitters for applications in chiral materials science, such as in CP Organic Light-Emitting Diodes (CP-OLEDs), optical information processing, bio-imaging or chiral sensing.[6-13] Transition metal- or lanthanide-based complexes were demonstrated to be strong candidates for applications in biological imaging, or for incorporation into CP-OLEDs due to their high CPL activity, efficient phosphorescence, or long-lived emission.[14,15] Despite the recent technical developments, the excited state properties still need to be characterized in terms of the electronic and structural

parameters that influence CPL activity at the molecular and supramolecular levels, and how the external medium, *i.e.* solvent and/or solid matrix may impact them. For example, the nature of the excited states involved in the CP emission is heavily influenced by the presence of transition metals or heavier elements. For chiral organic fluorophores, the first singlet excited state is generally responsible for the CP emission. In transition metal complexes, a triplet excited state is usually involved. For heavier elements such as the lanthanides, the emission is highly dependent on the intrinsic characteristics of the ion used (multiple and finely structured long-lived emission bands).[14,15] These considerations are particularly relevant in CP-OLEDs, in which both singlet and triplet excitons are electrically formed, and sometimes interconvert, before the electroluminescence takes place.

Recording both fluorescence and phosphorescence emission in the very same conditions for a given compound still represents a challenge due to the different timeframes and intensities for the processes. Helicenes, ortho-fused π-conjugated helical chromophores, have emerged as suitable candidates for CP-OLEDs and related devices due to their strong chiroptical activity. They not only display large optical rotation (OR) values and strong electronic circular dichroism (ECD) spectra, but they also exhibit intense CPL activity, with high emission dissymmetry factors surpassing 10^{-2} at the molecular level, a quite strong value for chiral organic chromophores (for reviews on CPL-active helicenes see references 16-19). In addition, due to their helical topology, helicenes display strong spin-orbit coupling, which enables efficient singlet to triplet intersystem crossing rates.[20-22] This feature has important consequences on the photophysics of this class of chiral chromophores: i) at room temperature the fluorescence quantum yields of carbo[*n*]helicene derivatives are usually modest (*ca.* 10% for carbo[6]helicene), ii) it is very often possible to

observe concomitantly fluorescence and phosphorescence signals at low temperature, *i.e.* 77 K,[23-25] *iii*) other energy transfer pathways such as singlet oxygen production may easily occur.[26]

Recently, our group reported the synthesis and chiroptical properties of a new family of π-helical push-pull systems based on 2,15-bis-ethynyl-carbo[6]helicene substituted by electron acceptor (4-pyridyl, 4-nitrophenyl, 4-cyanophenyl, shown on the left of Figure 1) or donor units (trimethylsilyl, dimethylamino, amino, see the right side of Figure 1) , and exhibiting strong CP fluorescence at room temperature with g_{lum} values up to 3-4 $\times$ 10^{-2} (g_{lum} = 2×(I_L-I_R)/(I_L+I_R), where I_L and I_R are intensities of emitted left-handed and right-handed circularly polarized lights, respectively).[27-33] In these systems, the optimal mutual orientation of the electric and magnetic dipoles in the excited-state enables helicene-mediated exciton coupling, which is a major contribution to the observed strong CP fluorescence.[27] This situation could be translated into an optoelectronic device, with the fabrication of a top-emission CP-OLEDs emitting electroluminescence dissymmetry factors g_{El} of 8×10^{-3}.[27]

In the present study, we take advantage of the unique synergy between the photophysical and intense chiroptical properties of these systems to explore the impact of the singlet/triplet spin state on the CP emission process. Indeed, in addition to the classical CP fluorescence observed at room temperature, CP phosphorescence, i.e. triplet state CP emission, can be also characterized at the molecular level in isotropic rigid matrix and at low temperature. This gave us a unique opportunity to directly compare the chirality of the singlet and triplet excited states through CPL emission, rationalized by a combination of experimental and theoretical studies.

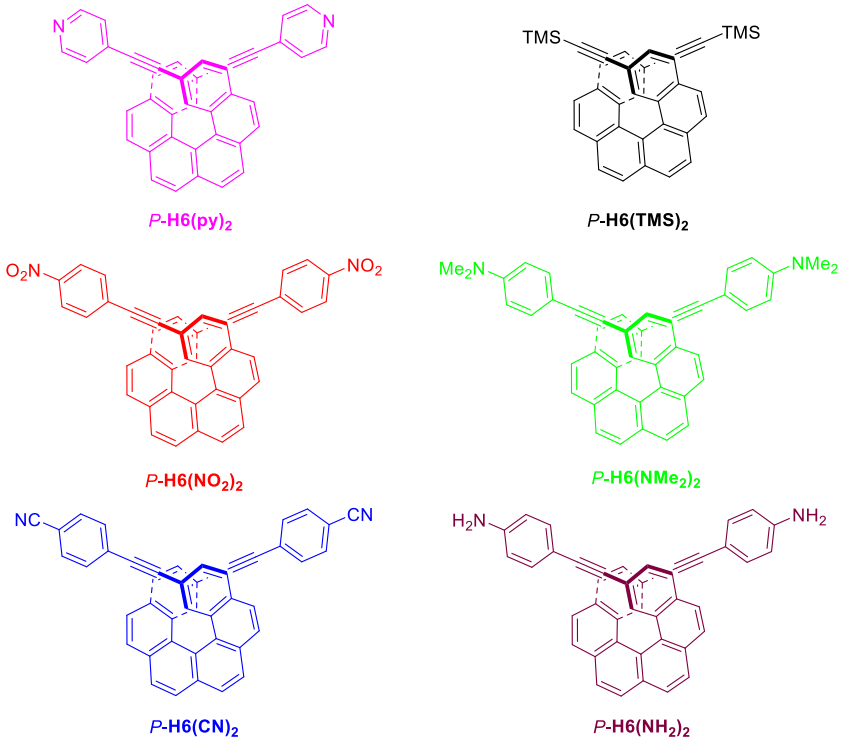

Figure 1. Chemical structures of enantiopure push-pull type π-helical molecules consisting of 2,15-bis-ethynyl-carbo[6]helicenes substituted with either electron acceptors (**H6(CN)$_2$**, **H6(py)$_2$**, and **H6(NO$_2$)$_2$**) or donors (**H6(TMS)$_2$**, **H6(NMe$_2$)$_2$**, and **H6(NH$_2$)$_2$**).

The room temperature luminescence and chiroptical properties of the push-pull helicene derivatives have been already reported (see Ref. 27) and are detailed in the Supporting Information.

Figure 2 shows the low-temperature emission spectra of the helicene-ethynyls substituted with electron acceptors (4-Ph-CN, 4-py and 4-Ph-NO_2) and electron donors (TMS, NMe_2 and NH_2) recorded at concentrations around 10^{-4} M, at 77 K in a frozen isotropic 2-MeTHF medium, see SI for further details.[34] For all compounds, two structured luminescence responses can be identified between 400 and 530 nm and between 530 and 700 nm, corresponding to fluorescence and phosphorescence emissions, respectively, as indicated by the recorded lifetimes of these process, which are in the order of few nanoseconds for the high energy emission and around 1 s for the low energy one (Table 1 and SI), and by theoretical calculations. Both fluorescence and phosphorescence signals are highly structured and present a vibronic progression of around 1300 cm^{-1} and 1600 cm^{-1}, respectively, except for the case of **H6(NO_2)$_2$**, in which the fluorescence response appears broader. This can be explained by the strong electron-withdrawing nature of the Ph-NO_2 substituent, which induces a higher charge-transfer character of the emission transition than in the other derivatives, as indicated by the observed solvatochromism of its room temperature fluorescence in DCM and 2-MeTHF solvents due to different polarities (Figure S1.33).

Time-gated emission measurement allowed to isolate the longer-lived phosphorescence signals more specifically (Figure 2), which display at least three clear vibronic lines for all systems. The exact values for emission wavelengths, vibronic effects and lifetimes are reported in Table 1. The similarity observed between the obtained signals suggest that the lowest excited triplet state responsible for the emission is mainly localized on the helicene core, with a limited impact of the substituents as confirmed by theoretical calculations (*vide infra*). However, one can clearly

visualize that the relative intensity between the fluorescence and phosphorescence emissions are different among the investigated compounds, with a high ratio in favor of the fluorescence emission for the donor-substituted helicenes **H6(NMe$_2$)$_2$** and **H6(NH$_2$)$_2$**, and to a less extent for **H6(CN)$_2$** and **H6(py)$_2$**. Interestingly, the presence of the nitro group reverses this ratio for **H6(NO$_2$)$_2$**, and the phosphorescence signal becomes much stronger than the fluorescence and it is characterized by a lifetime of about 0.46 s, substantially reduced in comparison to the measured phosphorescence lifetimes for the other derivatives. This can be explained by the enhanced spin-orbit coupling induced by the nitro group, allowing for a more efficient inter-system crossing between singlet and triplet states as shown by the calculated spin-orbit matrix elements reported in Section S2 of the Supporting Information.

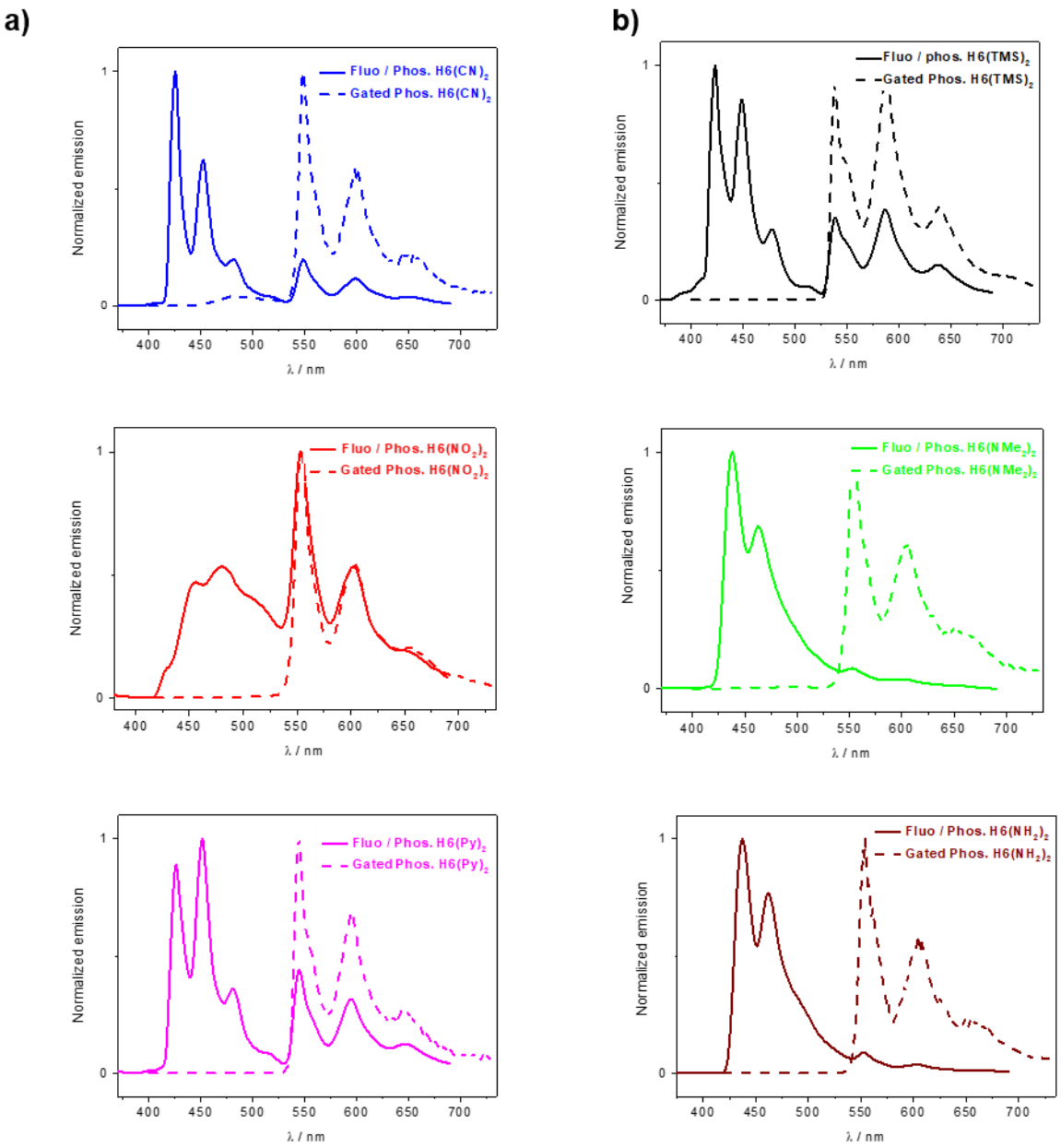

Figure 2. Low temperature full emission and time-gated spectra for π-helical a) acceptor and b) donor derivatives (77K in 2-MeTHF, excitation wavelength 375 nm).

Table 1. Photophysical data of compounds **H6(TMS)$_2$**, **H6(NO$_2$)$_2$**, **H6(CN)$_2$**, **H6(py)$_2$**, **H6(NH$_2$)$_2$**, and **H6(NMe$_2$)$_2$** in 2-Methyltetrahydrofuran at 77 K.

	***P*-H6(CN)$_2$**	***P*-H6(py)$_2$**	***P*-H6(NO$_2$)$_2$**
λ_{em}[a] (nm) / ΔE_{ST}[b]	425$_{Fl}$, 452$_{Fl}$, 481 $_{Fl}$, 514 $_{Fl}$, 553$_{Ph}$, 600 $_{Ph}$ / 0.67	425$_{Fl}$, 451$_{Fl}$, 481 $_{Fl}$, 512 $_{Fl}$, 545$_{Ph}$, 595 $_{Ph}$, 650 $_{Ph}$ / 0.66	456$_{Fl}$, 482$_{Fl}$, 513 $_{Fl}$, 553$_{Ph}$, 595 $_{Ph}$, 650 $_{Ph}$ / 0.62
τ_{Fluo}[c] [ns]	22	22	2.6 (67%) & 0.85 (32%)
$\tau_{Phos.}$[d] [s]	0.98	1.1	0.46
$\lvert g_{Fluo}\rvert$ at λ (nm)	1.5×10^{-2} (425)	1.9×10^{-2} (420)	0.8×10^{-2} (482)
$\lvert g_{phos.}\rvert$ at λ (nm)	-0.4×10^{-2} (540)	-0.37×10^{-2} (540)	-1.6×10^{-2} (553)
	***P*-H6(TMS)$_2$**	***P*-H6(NMe$_2$)$_2$**	***P*-H6(NH$_2$)$_2$**
λ_{em}[b] (nm) / ΔE_{ST}[c]	423$_{Fl}$, 450$_{Fl}$, 480 $_{Fl}$, 537 $_{Ph}$, 589$_{Ph}$, 640 $_{Ph}$ / 0.67	438$_{Fl}$, 464$_{Fl}$, 488 $_{Fl}$, 554$_{Ph}$, 601 $_{Ph}$, 650 $_{Ph}$ / 0.64	437$_{Fl}$, 464$_{Fl}$, 488 $_{Fl}$, 554$_{Ph}$, 601 $_{Ph}$, 650 $_{Ph}$ / 0.64
τ_{Fluo}[b] [ns]	22 (95%) & 5.1 (5%)	6.5 (59%) & 12.6 (41%)	7.5 (20%) & 11.5 (80%)
$\tau_{Phos.}$[b] [s]	1.1	0.88	0.85
$\lvert g_{Fluo}\rvert$ at λ (nm)	0.5×10^{-2} (425)	1.3×10^{-2} (441)	1.8×10^{-2} (433)
$\lvert g_{Phos}\rvert$ at λ (nm)	-0.2×10^{-2} (540)	–	–

[a] In 2-MeTHF ($\sim 10^{-5}$ M) with λ_{ex} = 375 nm [b] Determined from the onset of fluorescence and gated phosphorescence spectra [c] Fluorescence lifetimes (error ± 5%) the two component decays are given (weight in parenthesis). [d] Triplet-state lifetimes in 2-MeTHF with λ_{ex} = 360 nm and gate = 99 ms

The low temperature experimental CPL of the helicene-ethynyls derivatives were also recorded in conditions similar to the unpolarized emission spectra (Figure 3). *Quasi*-mirror-image CPL spectra were obtained for all emitters, which demonstrates that the signals arise from the chiral emitters and not from potentials artifacts related to the frozen medium (see the Supporting Information for details). It is important to note that the frozen medium may introduce some inhomogeneity that should be considered with much care for analyzing the experimental data. Indeed, it is known that CPL measurements in the solid state may be contaminated by other contributions including anisotropic effects (such as linear birefringence and linear dichroism).[35] For this reason, the influence of such effects were verified in the case of **H6(TMS)$_2$** by rotating the sample by 90° (see Figure S1.32 in the Supporting Information for a picture of the cooling system and of the NMR tube used for the measurements). Although minor differences were observed, the similarity of the

fluorescence signal that was already known at room temperature ascertains the consistency of our measurements.

For all compounds, the CPL shows maxima corresponding to those obtained for the unpolarized spectra, notably with the presence of CP fluorescence positive signals for the *P* enantiomers and negative ones for the *M* enantiomers in full agreement with our previously reported results on CPL observed at room temperature (see ref. 27). While for the three donor substituted compounds **H6(NMe$_2$)$_2$**, **H6(NH$_2$)$_2$** and **H6(TMS)$_2$** CPL can be detected only between 420 and 500 nm, *i.e.* in the fluorescence domain (except a weak response around 550 nm for **H6(TMS)$_2$**), clear structured CP phosphorescence signals between 520 and 650 nm are unambiguously observed for **H6(CN)$_2$**, **H6(py)$_2$**, and **H6(NO$_2$)$_2$**, in accordance with the already mentioned unpolarized phosphorescence (Figure 3). Surprisingly, these low energy CP signals are inverted in sign compared to CP fluorescence (i.e. negative for the *P* and positive for the *M* enantiomers, with g_{lum} of -0.4×10^{-2}, -0.37×10^{-2} and -1.6×10^{-2} for *P*-**H6(CN)$_2$**, *P*-**H6(py)$_2$**, and *P*-**H6(NO$_2$)$_2$**, respectively, at the stronger emission lines, see Table 1 and SI) and appeared rather intense for **H6(NO$_2$)$_2$** which exhibits around 1.5 times higher phosphorescence g_{lum} as compared to the fluorescence dissymmetry factor (-0.75×10^{-2} for *M*-**H6(NO$_2$)$_2$**). The similar structured CP phosphorescence obtained for these three compounds is another evidence of their common origin, namely the carbo[6]helicene backbone, as already indicated by the unpolarized photophysical characterization. Therefore, these systems provide a rare case in which CP fluorescence and phosphorescence can be observed under similar conditions at the molecular level, thus enabling the direct comparison between the singlet and triplet excited-state CP emission in terms of sign for a purely organic emitter.

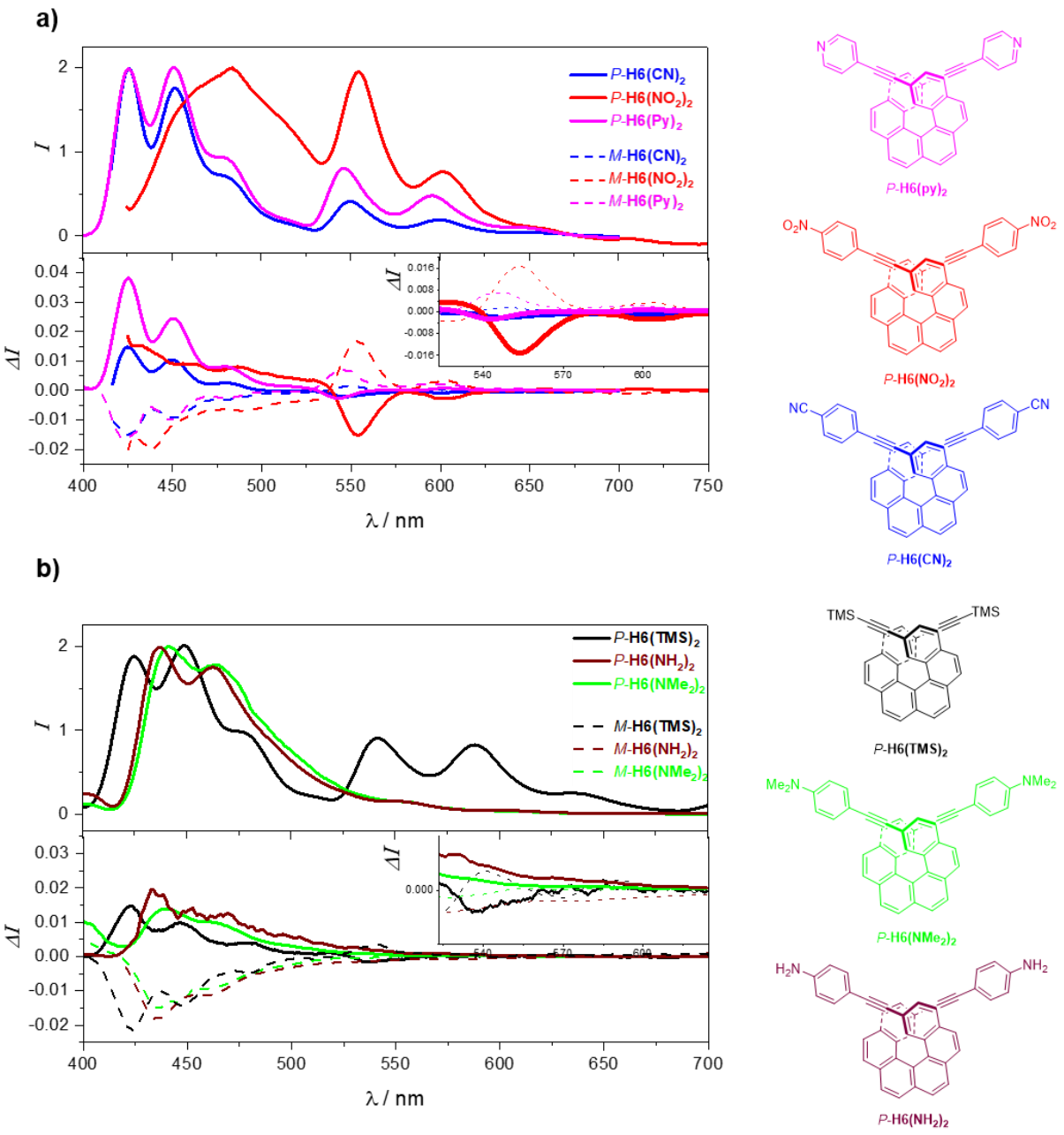

Figure 3. Low temperature emission (top) and CPL (bottom) spectra of 2,15-ethynyl-carbo[6]helicene systems with a) electron acceptors **H6(CN)$_2$**, **H6(NO$_2$)$_2$**, **H6(py)$_2$** and b) electron donors **H6(TMS)$_2$**, **H6(NMe$_2$)$_2$**, **H6(NH$_2$)$_2$**. Inserts: CPL responses in selected domains 500-680 nm. All the spectra were recorded at 77k in 2-MeTHF solution and excitation at 375 nm.

The experimental CPL spectra and calculated vibrationally resolved CPL for the S_1–S_0 emission of *P*-**H6(py)$_2$** and *P*-**H6(NO$_2$)$_2$** are shown in Panels **A** and **B** of Figure 4. Corresponding results for the *P*-**H6(NMe$_2$)$_2$** and *P*-**H6(TMS)$_2$** compounds are shown in Panels **A** and **B** of Figure 5. The *P*-isomers of the compounds were considered for the theoretical analysis; therefore, this notation is omitted in the following discussion. The calculated spectra were shifted by –0.38 eV to align the most intense peaks with the experimental spectra, as commonly done. Overestimation of helicene transition energies with the chosen functional (CAM-B3LYP) by about 0.4 eV is not uncommon and has been noted in related previous research.[10] After the shift, the calculated and measured fluorescence CPL for **H6(py)$_2$**, **H6(NMe$_2$)$_2$**, and **H6(TMS)$_2$** are in excellent agreement. For **H6(NO$_2$)$_2$**, the experimental fluorescence spectrum is not as well resolved. For consistency between the calculations, the same broadening of the transitions was used for all systems, although it appears that a larger broadening should be used for **H6(NO$_2$)$_2$** to reproduce the weakly structured CPL observed between ca. 440 and 520 nm. Although the CPL spectrum of **H6(NMe$_2$)$_2$** appears less resolved than those of **H6(py)$_2$** and **H6(TMS)$_2$**, a similar peak structure is observed. The calculated spectra exhibit the same pattern, which constitute vibrational progressions with the most intense bands at low wavelengths from the 0-0 transitions.

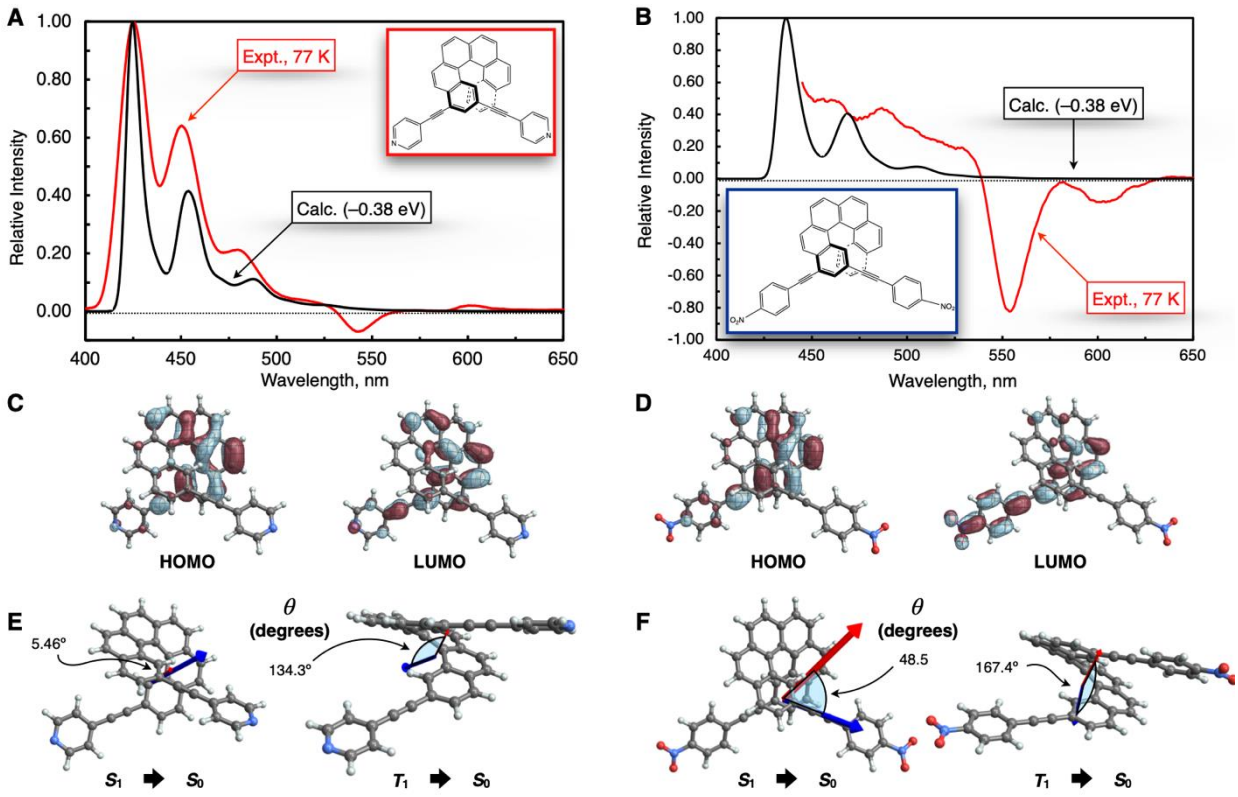

Figure 4. Calculated (black curves) and experimental (red curves) S_1–S_0 CPL spectrum of *P*-**H6(py)$_2$** (left, panel A; the structure is shown in the red insert) and *P*-**H6(NO$_2$)$_2$** (right, panel B; the structure is shown in the blue insert). Panels C and D show selected molecular orbitals of the U-DFT-optimized triplet excited state structure for both species (±0.03 isosurfaces). The molecular orbitals for the S_1 and S_0 structures are qualitatively similar (see Supporting Information). Panels E and F show electric (red arrows) and magnetic (blue arrows) transition dipole moments, arbitrarily scaled relative to the images of the U-DFT T_1 geometry, with the angle (in degrees) between them for the S_1–S_0 and T_1–S_0 transition, respectively.

Around 550 nm, all molecules show phosphorescence, with emission lifetimes of about 8 orders of magnitude larger than the fluorescence (Table 2). Accordingly, the peaks are assigned to emission from the lowest triplet state, T_1. The T_1 emission data were calculated separately and are

therefore not contained in the calculated spectra shown in Figures 4 and 5. A summary of calculated and experimental photophysical data is provided in Table 2. The calculations confirm T_1 emission, with T_1–S_0 energies calculated in the same range where the most intense negative CPL bands appear (albeit somewhat underestimated in energy). The S_1–S_0 and the T_1–S_0 emissions involve predominantly the pair of highest occupied and lowest unoccupied molecular orbitals (HOMO and LUMO, see panels **C** and **D** of Figures 3 and 4). In agreement with the experiments, the triplet emission for the *P* enantiomers is calculated to have negative rotatory strength, opposite to the singlet emission. The calculated and experimental g_{lum} have comparable orders of magnitude. As already mentioned earlier, the molecular orbitals involved in the S_1–S_0 and the T_1–S_0 transitions are localized on the helicene core, with additional minor contributions from the substituents in the case of **H6(NMe$_2$)$_2$** and **H6(NO$_2$)$_2$**.

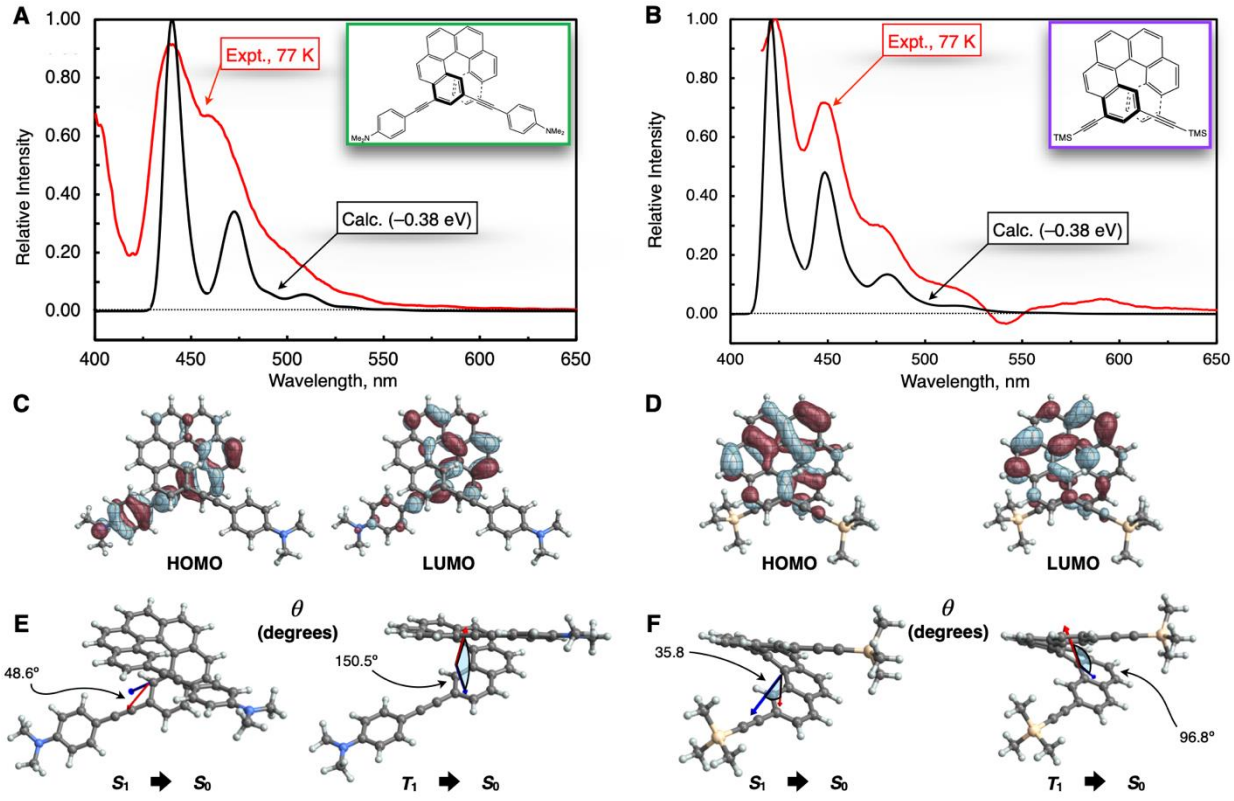

Figure 5. Calculated (black curves) and experimental (red curves) S_1–S_0 CPL spectrum of **H6(NMe$_2$)$_2$** (left, panel A; the structure is shown in the green insert) and **H6(TMS)$_2$** (right, panel B; the structure is shown in the purple insert). Panels C and D show selected molecular orbital of the U-DFT-optimized triplet excited state structures. Panels E and F show electric (red arrows) and magnetic (blue arrows) transition dipole moments, arbitrarily scaled relative to the images of the U-DFT T_1 geometry. See caption of Figure 3 for additional details.

The calculations agree with the experiments on fluorescence emission lifetimes in the nano- to ten nano-second range. For the spin-forbidden triplet transitions causing the phosphorescence, the calculated lifetimes have the right order of magnitude, although they overestimate the experimental values. The calculated lifetime is very sensitive to the energy used for the calculation, as pointed out in the Computational Details below and in Section 2 of the Supporting Information, and it is

likely that the calculated dipole strengths for the triplet emission are underestimated, causing the lifetimes to be somewhat too high. Furthermore, the calculations do not model dynamic processes that may lead to decreased phosphorescence lifetimes, nor do they mimic the inhomogeneity effects that are due to the frozen medium. Overall, the calculations are in satisfactory, semi-quantitative agreement with the experiments and confirm that the CPL bands observed at low temperature around 550 nm can be assigned to T_1–S_0 emission, with rotatory strengths opposite to the S_1–S_0 emission and lifetimes differing by factors of 10^8 to 10^9.

Table 2. The calculated rotatory strengths (R), the experimental and calculated dissymmetry factors for CPL emission (g_{lum}), and the experimental and calculated lifetimes.

Molecule	State	Energy, *calc*[a]	Energy, after shifting[a]	R[b]	$\lvert g_{lum}\rvert$, *expt.*	$\lvert g_{lum}\rvert$, *calc*[c]	Lifetime expt.[d]	Lifetime in 2-MeTHF[d,e]
H6(py)$_2$	T_1	1.94	2.29	-1.44×10^{-5}	3.7×10^{-3}	2.3×10^{-2}	1.1	3.07
	S_1	3.31	2.93	1.29×10^{2}	1.9×10^{-2}	3.3×10^{-2}	2.2×10^{-8}	7.85×10^{-8}
H6(NO$_2$)$_2$	T_1	1.97	2.24	-1.50×10^{-5}	1.6×10^{-2}	2.0×10^{-2}	0.46	2.74
	S_1	3.25	2.87	1.22×10^{3}	8.0×10^{-3}	1.3×10^{-2}	2.6×10^{-9}	3.38×10^{-9}
H6(TMS)$_2$	T_1	1.98	2.29	-1.03×10^{-5}	2.0×10^{-3}	2.0×10^{-2}	1.1	3.69
	S_1	3.33	2.95	2.62×10^{1}	5.0×10^{-3}	3.5×10^{-2}	2.2×10^{-8}	3.99×10^{-7}
H6(NMe$_2$)$_2$	T_1	1.95	2.22	-1.39×10^{-5}	N/A	1.9×10^{-2}	0.88	2.83
	S_1	3.22	2.84	1.18×10^{3}	1.3×10^{-2}	1.2×10^{-2}	6.5×10^{-9}	3.51×10^{-9}

[a] In units of eV; [b] Calculated in cgs units of 10^{-40} esu^2 cm^2. For triplet states: Sum of rotatory strengths of triplet components. [c] Calculated as $4R$ / D. Dimensionless. For triplet states, R and D are averaged over triplet components. [d] In units of seconds. [e] Inverses of emission rates calculated using the shifted energies which correspond to the experimental band peak maxima (0-0 for the fluorescence). Rates for triplet components were averaged. To obtain the values, the lifetimes calculated in vacuum were divided by the square of the refractive index of the solvent (1.408).[36]

Tables S2.18, S2.20, S2.22, and S2.24 show that for the four compounds considered for the theoretical analysis, the S_1 state is higher in energy than at least three triplet states (five for the

nitro-substituted compound), making the ISC energetically favored. It can therefore be assumed that ISC involves one of the higher triplet states, followed by relaxation to T_1 through internal conversion. Further analysis of the spin-orbit (SO) coupling strengths between pure spin states showed that the SO interaction mixes singlets S_0 and S_2 each predominantly with T_1, and furthermore it mixes triplets T_3, and T_4 each with S_0. The dipole and rotatory strengths of the spin-forbidden transition T_1–S_0 arise entirely from this mixing of triplets into S_0 and mixing of singlets into T_1. CPL of the same sign and same assignment as for the S_1–S_0 emission would only be expected if the main source of intensity for T_1–S_0 emission were an admixture of S_1 into T_1. However, S_1 and T_1 are assigned to the same HOMO-LUMO transition and therefore the two states have the same symmetry. According to the El-Sayed rule,[37] then, the SO interaction does not mix them in first order. Figures 4 and 5, panels **E** and **F** indicate the orientations of the calculated electric **d** and magnetic **m** transition dipole vectors relative to the molecular frame. The rotatory strength is $R = \mathrm{Im}[\mathbf{d}\ \mathbf{m}^*]$, therefore what is shown in the figure corresponds to $\mathrm{Im}[\mathbf{m}^*]$. The angles of less than 90 deg in the S_1–S_0 transitions are consistent with the positive CPL for the *P* enantiomers, as the dot product is proportional to the angle's cosine. The transition dipole vectors for the triplet emission do not resemble those for the singlet emission, because they represent linear combinations of singlet-singlet and triplet-triplet transition dipoles other than the HOMO-LUMO transition caused by the SO-induced mixing of spin states. The rotatory strengths for T_1–S_0 then happens to be negative for the *P* enantiomers.

In this work, the origin of the low-temperature circularly polarized emission of six helicene-based molecules is reported with extensive experimental and theoretical analysis. The six compounds examined have electron-donating and electron-withdrawing groups, resulting in a wide range of dissymmetry factors and fluorescence and phosphorescence lifetimes. The nitro-substituted helicene exhibits the strongest phosphorescence, and it is the ideal candidate for CPL-based applications. Theoretical analysis has shown that the rotatory strength is opposite in sign for the singlet and triplet emission processes, in agreement with the experiments. The exceptional properties of the nitro-substituted compound are due to an efficient inter-system crossing originating in singlet-triplet admixtures that involve higher singlet and triplet states but exclude the direct mixing of S_1 and T_1, as quantified through the calculated spin-orbit matrix elements. The calculations also show that the triplet state is mostly localized on the helicene core, with little influence from the substituents. This work is among the first account of low temperature CPL measurements,[52,53] and it paves the way toward the direct characterization of the triplet excited state of organic CPL emitters.

All calculations employed the Kohn–Sham density functional theory (KS DFT) and the time-dependent DFT (TD-DFT) linear response methods. Geometry optimizations and vibrational frequency calculations with the CAM-B3LYP functional[38] and the def2-SV(P) Gaussian-type basis set[39] were performed with Gaussian 16 (G16).[40] Vibrationally resolved singlet emission and CPL spectra including Franck-Condon and Herzberg-Teller effects were calculated as implemented in G16.[41] The vibronic transitions were Gaussian broadened with a sigma of 0.0248 eV to obtain the calculated spectra shown in Figures 3 and 4, Panels **A** and **B**. For general

overviews of TD-DFT approaches to calculating natural optical activity, see also References 42 and 43.

Triplet emission lifetimes and dipole strengths were determined from TD-DFT calculations including the spin-orbit interaction.[36,44-46] These calculations used the 2021 release of the Amsterdam Density Functional (ADF) program.[47] The CAM-B3LYP functional, the DZP (DZ on hydrogens) Slater-type basis sets,[48] and the zeroth-order regular approximation (ZORA) two-component relativistic Hamiltonian were employed for these calculations. Magnetic transition dipole moments and rotatory strengths for the T_1-S_0 transitions were obtained with a recent modification of ADF,[44] implementing the CDSPECTRUM keyword for SO-TDDFT calculations. This code is available since the 2021 release and will be documented in detail in future releases. Additional calculations were conducted with the ORCA program[49] to obtain matrix elements for the spin-orbit interaction between singlet and triplet states, to gauge qualitatively which states couple the strongest. Emission rates k were calculated according to Reference 36.

$$\boldsymbol{k = \frac{4}{3}\alpha^3 E^3 D} \quad (1)$$

In Equation 1, E is the energy for a transition, D its dipole strength, both in atomic units, and α is the fine structure constant. The emission lifetime is $1/k$, which is then converted from atomic units to seconds. The calculated zero-field splitting (ZFS) of T_1 for all compounds investigated is negligible, such that the transition rates for the triplet components can simply be averaged prior to conversion to the lifetime. Because of the factor E^3 in Equation 1, small errors in the energies translate into large errors in the lifetimes, and therefore we used the experimental band peak energies to calculate phosphorescence lifetimes and shifted singlet 0-0 energies for the fluorescence lifetimes. As shown in Reference 36, when the ZFS is appreciable, the rates should be Boltzmann-averaged. In all cases, TD-DFT calculations for the triplet states employed the

Tamm-Dancoff approximation (TDA),[50] to avoid the triplet near-instability as noted previously by Peach et al.[51] For additional computational details, please see the Supporting Information.

Associated Content

Supporting Information. The following files are available free of charge.

Additional details on the experimental procedures, and additional pictures of the recorded spectra for all compounds are presented in Section 1 of the Supporting Information document.

Additional computational details, benchmark calculations for the excitation energies, spin-orbit coupling matrix elements, pictures of the orbitals, and molecular geometries in xyz format are collected in Section 2 of the Supporting Information (LowTemCPL_SI.docx).

Author Information

Corresponding Authors:

J. Autschbach - Department of Chemistry, University at Buffalo, State University of New York, Buffalo, NY 14260, USA. ORCID: 0000-0001-9392-877X; E-mail: jochena@buffalo.edu

L. Favereau - Univ Rennes, CNRS, ISCR-UMR 6226, ScanMAT–UMS 2001, F-35000 Rennes, France. ORCID: 0000-0001-7847-2911 ; E-mail: ludovic.favereau@univ-rennes1.fr

J. Crassous - Univ Rennes, CNRS, ISCR-UMR 6226, ScanMAT–UMS 2001, F-35000 Rennes, France. ORCID: 0000-0002-4037-6067; E-mail: jeanne.crassous@univ-rennes1.fr

Authors:

K. Dhbaibi - Univ Rennes, CNRS, ISCR-UMR 6226, ScanMAT–UMS 2001, F-35000 Rennes, France. ORCID: 0000-0001-7830-6913

P. Morgante - Department of Chemistry, University at Buffalo, State University of New York, Buffalo, NY 14260, USA. ORCID: 0000-0002-7522-2535

N. Vanthuyne - Aix Marseille University, CNRS Centrale Marseille, iSm2, 13284 Marseille, France. ORCID: 0000-0003-2598-7940

Notes

The authors declare no competing financial interest.

Acknowledgements

We acknowledge the Ministère de l'Education Nationale, de la Recherche et de la Technologie, the Centre National de la Recherche Scientifique (CNRS). J.A. thanks the National Science Foundation for financial support of the theoretical component of this research from grant CHE-2152633. P.M. and J.A. acknowledge the Center for Computational Research (CCR) at the University at Buffalo for providing computational resources.

References

(1) Riehl, J. P.; Richardson, F. S. Circularly Polarized Luminescence Spectroscopy. *Chem. Rev.* **1986**, *86*, 1–16.
(2) Dekkers, H. P. J. M. in: Berova, N.; Nakanishi, K.; Woody, R. W.Circular Dichroism, Principles and Applications, Wiley-VCH, New York, **2000**.
(3) Longhi, G.; Castiglioni, E.; Koshoubu, J.; Mazzeo, G.; Abbate, S. Circularly Polarized Luminescence: A Review of Experimental and Theoretical Aspects. *Chirality* **2016**, *28*, 696–707.
(4) Meskers, S. C. J. Circular Polarization of Luminescence as a Tool To Study Molecular Dynamical Processes. *ChemPhotoChem* **2022**, *6*, e20210015.
(5) Mori, T. Circularly Polarized Luminescence of Isolated Small Organic Molecules », Springer, **2020**, pp 53–97.
(6) Steinberg, I. Z. Circular Polarization of Luminescence: Biochemical and Biophysical Applications. *Ann. Rev. Biophys. Bioeng.* **1978**, *7*, 113–137.
(7) Wang, H.; Liu, L.; Lu, C. CPLC: Visible Light Communication based on Circularly Polarized Light. *Procedia Comput. Sci.* **2018**, *131*, 511–519.
(8) Han, J. M.; Guo, S.; Lu, H.; Liu, S. J.; Zhao, Q.; Huang, W. Recent Progress on Circularly Polarized Luminescent Materials for Organic Optoelectronic Devices. *Adv. Opt. Mater.* **2018**, *6*, 1800538.
(9) Novikova, T.; Pierangelo, A.; Manhas, S.; Benali, A.; Validire, P.; Gayet, B.; Martino, A. D. Circular Polarization in Nature: Factual, Theoretical and Experimental Summary. *Appl. Phys. Lett.* **2013**, *102*, 241103.
(10) Kunnen, B.; Macdonald, C.; Doronin, A.; Jacques, S.; Eccles, M.; Meglinski, I. Application of Circularly Polarized Light for Non-Invasive Diagnosis of Cancerous Tissues and Turbid Tissue-Like Scattering Media. *J. Biophotonics* **2015**, *8*, 317–323.
(11) Zhang, D. W.; Li, M.; Chen, C. F. Recent Advances in Circularly Polarized Electroluminescence Based on Organic Light-Emitting Diodes. *Chem. Soc. Rev.* **2020**, *49*, 1331–1343.
(12) Brandt, J. R.; Wang, X.; Yang, Y.; Campbell A. J.; Fuchter, M. J. Circularly Polarized Phosphorescent Electroluminescence with a High Dissymmetry Factor from PHOLEDs Based on a Platinahelicene. *J. Am. Chem. Soc.* **2016**, *138*, 9743–9746.
(13) MacKenzie, L. E.; Pal, R. Circularly polarized lanthanide luminescence for advanced security inks. *Nat. Rev. Chem.* **2021**, *5*, 109–124.
(14) Carr, R.; Evans, N. H.; Parker, D. Lanthanide Complexes as Chiral Probes Exploiting Circularly Polarized Luminescence. *Chem. Soc. Rev.* **2012**, *41*, 7673–7686.
(15) Doistau, B.; Jiménez J.-R.; C. Piguet, C. Beyond Chiral Organic (p-Block) Chromophores for Circularly Polarized Luminescence: The Success of d-Block and f-Block Chiral Complexes. *Front. Chem.* **2020**, *8*, 555.
(16) Zhao, W.-L.; Li, M.; Lu, H.-Y.; Chen, C.-F. Advances in Helicene Derivatives With Circularly Polarized Luminescence. *Chem. Commun.* **2019**, *55*, 13793–13803.
(17) J. Crassous in "Circularly Polarized Luminescence of Isolated Small Organic Molecules", T. Mori (ed.), Springer, **2020**, chap. 4, pp 53–97.
(18) Dhbaibi, K.; Favereau, L.; Crassous, J. Enantioenriched Helicenes and Helicenoids Containing Main-Group Elements (B, Si, N, P). *Chem. Rev.* **2019**, *119*, 8846–8953.
(19) J. Crassous, J.; Stará, I. G.; Starý, I. Helicenes - Synthesis, Properties and Applications, Wiley, **2022**.

(20) Sapir, M.; Donckt, E. V., Intersystem Crossing in the Helicenes. *Chem. Phys. Lett.* **1975,** *36*, 108–110.
(21) Nijegorodov, N. I.; Downey, W. S., The Influence of Planarity and Rigidity on the Absorption and Fluorescence Parameters and Intersystem Crossing Rate Constant in Aromatic Molecules. *J. Phys. Chem.* **1994,** *98*, 5639–5643.
(22) Nagarajan, K.; Mallia, A. R.; Muraleedharan K.; Hariharan, M. Enhanced Intersystem Crossing in Core-Twisted Aromatics. *Chem. Sci.* **2017**, *8*, 1776–1782.
(23) Norel, L.; Rudolph, M.; Vanthuyne, N.; Williams, J. A. G.; Lescop, C.; Roussel, C.; Autschbach, J.; Crassous, J.; Réau, R. Metallahelicenes: A Novel Family of Easily Accessible Helicene Derivatives Exhibiting Important and Tuneable Chiroptical Properties. *Angew. Chem. Int. Ed.* **2010**, *49*, 99–102.
(24) Shen, C.; Anger, E.; Srebro, M.; Vanthuyne, N.; Deol, K. K.; Jefferson Jr., T. D.; Muller, G.; Williams, J. A. G.; Toupet, L.; Roussel, C.; Autschbach, J.; Réau, R.; Crassous, J. Straightforward Access to Mono- and Bis-Cycloplatinated Helicenes That Display Circularly Polarized Phosphorescence Using Crystallization Resolution Methods. *Chem. Sci*. **2014,** *5*, 1915–1927.
(25) Shen, C.; Srebro-Hooper, M.; Jean, M.; Vanthuyne, N.; Toupet, L.; Williams, J. A. G.; Torres, A. R.; Riives, A. J.; G. Muller, G.; Autschbach, J.; Crassous, J. Synthesis and Chiroptical Properties of Hexa-, Octa- And Deca-Azaborahelicenes: Influence of the Helicene's Size and of the Number of Boron Atoms. *Chem. Eur. J.* **2017**, *23*, 407–418.
(26) Galland, M.; Riobé, F.; Ouyang, J.; Saleh, N.; Pointillart, F.; Dorcet, V.; Le Guennic, B.; Cador, O.; Crassous, J.; Andraud, C.; Monnereau, C.; Maury, O**.** Helicenic Complexes of Lanthanides: Influence of the F-Element on the Intersystem Crossing Efficiency and Competition Between Luminescence and Oxygen Sensitization. *Eur. J. Inorg. Chem.* **2019**, 118–125.
(27) Dhbaibi, K.; Abella, L.; Meunier-Della-Gatta, S.; Roisnel, T.; Vanthuyne, N.; Jamoussi, B.; Pieters, G.; Racine, B.; Quesnel,E.; Autschbach, J.; Crassous, J.; Favereau, L. Achieving High Circularly Polarized Luminescence with Push-Pull Helicenic Systems: From Rationalized Design to Top-Emission CP-OLED Applications. *Chem. Sci.* **2021**, *12*, 5522–5533.
(28) Dhbaibi, K.; Favereau, L.; Srebro-Hooper, M.; Jean,M.; Vanthuyne, N.; Zinna, F.; Jamoussi, B.; Di Bari, L.; Autschbach J.; Crassous, J. Exciton Coupling in Diketopyrrolopyrrole-Helicene Derivatives Leads to Red and Near-Infrared Circularly Polarized Luminescence. *Chem. Sci.* **2018**, *9*, 735–742.
(29) Dhbaibi, K.; Favereau, L.; Srebro-Hooper, M.; Quinton, C.; Vanthuyne, N.; Arrico, L.; Roisnel, T.; Jamoussi, B.; Poriel, C.; Cabanetos, C.; Autschbach, J.; Crassous, J. Modulation of Circularly Polarized Luminescence Through Excited-State Symmetry Breaking and Interbranched Exciton Coupling in Helical Push-Pull Organic Systems. *Chem. Sci.* **2020**, *11*, 567–576.
(30) Bouvier, R.; Durand, R.; Favereau, L.; Srebro-Hooper, M.; Dorcet, V.; Roisnel, T.; Vanthuyne, N.; Vesga, Y.; Donnelly, J.; Hernandez, F.; Autschbach, J.; Trolez, Y.; Crassous, J. Helicenes Grafted With 1,1,4,4-Tetracyanobuta-diene Moieties: π-Helical Push-Pull Systems With Strong Electronic Circular Dichroism and Two-Photon Absorption. *Chem. Eur. J.* **2018**, *24*, 14484–14494.
(31) Shen, C.; Gan, F.; Zhang, G.; Ding, Y.; Wang, J.; Wang, R.; Crassous, J.; Qiu, H. Tunable Circularly Polarized Luminescence of Helicene-Derived Aggregation-Induced Emission Adducts. *Mater. Chem. Front.* **2020**, *4*, 837–844.

(32) Dhbaibi, K.; Matozzo, P.; Abella, L.; Jean, M.; Vanthuyne, N.; Autschbach, J.; Favereau, L.; Crassous, J. Exciton Coupling Chirality in Helicene-Porphyrin Conjugates. *Chem. Comm.* **2021**, *57*, 10743–10746.
(33) Rodríguez, R.; Naranjo, C.; Kumar, A.; Matozzo, P.; Das, T.-K.; Zhu, Q.; Vanthuyne, N.; Gómez, R.; Naaman, R.; Sánchez, L.; Crassous, J. Mutual Monomer Orientation to Bias the Supramolecular Polymerization of [6]Helicenes and the Resulting Circularly Polarized Light and Spin Filtering Properties. *J. Am. Chem. Soc.* **2022**, *144*, 7709–7719.
(34) Aycock, D. F. Solvent Applications of 2-Methyltetrahydrofuran in Organometallic and Biphasic Reactions. *Org. Process Res. Dev.* **2007**, *11*, 156–159.
(35) Albano, G.; Pescitelli, G.; Di Bari, L. Chiroptical Properties in Thin Films of π-Conjugated Systems. *Chem. Rev.* **2020**, *120*, 10145–10243.
(36) Mori, K.; Goumans, T. P. M.; Lenthe, E. van; Wang, F. Predicting Phosphorescent Lifetimes and Zero-Field Splitting of Organometallic Complexes with Time-Dependent Density Functional Theory Including Spin-Orbit Coupling. *Phys. Chem. Chem. Phys.* **2014**, *16*, 14523–14530.
(37) El-Sayed, M. A. The Radiationless Processes Involving Change of Multiplicity in the Diazenes. *J. Chem. Phys.* **1962**, *36*, 573–574.
(38) Yanai, T.; Tew, D. P.; Handy, N. C. A New Hybrid Exchange-Correlation Functional Using the Coulomb-Attenuating Method (CAM-B3LYP). *Chem. Phys. Lett.* **2004**, *393*, 51–57.
(39) Weigend, F.; Ahlrichs, R. Balanced Basis Sets of Split Valence, Triple Zeta Valence and Quadruple Zeta Valence Quality for h to Rn: Design and Assessment of Accuracy. *Phys. Chem. Chem. Phys.* **2005**, *7*, 3295–3305.
(40) Frisch, M. J.; Trucks, G. W.; Schlegel, H. B.; Scuseria, G. E.; Robb, M. A.; Cheeseman, J. R.; Scalmani, G.; Barone, V.; Petersson, G. A.; Nakatsuji, H.; Li, X.; Caricato, M.; Marenich, A. V.; Bloino, J.; Janesko, B. G.; Gomperts, R.; Mennucci, B.; Hratchian, H. P.; Ortiz, J. V.; Izmaylov, A. F.; Sonnenberg, J. L.; Williams-Young, D.; Ding, F.; Lipparini, F.; Egidi, F.; Goings, J.; Peng, B.; Petrone, A.; Henderson, T.; Ranasinghe, D.; Zakrzewski, V. G.; Gao, J.; Rega, N.; Zheng, G.; Liang, W.; Hada, M.; Ehara, M.; Toyota, K.; Fukuda, R.; Hasegawa, J.; Ishida, M.; Nakajima, T.; Honda, Y.; Kitao, O.; Nakai, H.; Vreven, T.; Throssell, K.; Montgomery, J. A., Jr.; Peralta, J. E.; Ogliaro, F.; Bearpark, M. J.; Heyd, J. J.; Brothers, E. N.; Kudin, K. N.; Staroverov, V. N.; Keith, T. A.; Kobayashi, R.; Normand, J.; Raghavachari, K.; Rendell, A. P.; Burant, J. C.; Iyengar, S. S.; Tomasi, J.; Cossi, M.; Millam, J. M.; Klene, M.; Adamo, C.; Cammi, R.; Ochterski, J. W.; Martin, R. L.; Morokuma, K.; Farkas, O.; Foresman, J. B.; Fox, D. J. Gaussian 16 Revision c.01.
(41) Santoro, F.; Lami, A.; Improta, R.; Bloino, J.; Barone, V. Effective Method for the Computation of Optical Spectra of Large Molecules at Finite Temperature Including the Duschinsky and Herzberg–Teller Effect: The Qx Band of Porphyrin as a Case Study. *J. Chem. Phys.* **2008**, *128*, 224311–224317.
(42) Srebro-Hooper, M.; Autschbach, J. Calculating Natural Optical Activity of Molecules From First Principles. *Annu. Rev. Phys. Chem.* **2017**, *68*, 399–420.
(43) Autschbach, J.; Nitsch-Velasquez, L.; Rudolph, M. Time-Dependent Density Functional Response Theory for Electronic Chiroptical Properties of Chiral Molecules. *Top. Curr. Chem.* **2011**, *298*, 1–98.
(44) Ludowieg, H. D.; Srebro-Hooper, M.; Crassous, J.; Autschbach, J. Optical Activity of Spin-Forbidden Electronic Transitions in Metal Complexes From Time-Dependent Density Functional Theory with Spin-Orbit Coupling. *ChemistryOpen* **2022**, *11*, e202200020.

(45) Marian, C. M. Spin–Orbit Coupling and Intersystem Crossing In Molecules. *WIREs Comput. Mol. Sci.* **2012**, *2*, 187–203.
(46) Egidi, F.; Fusè, M.; Baiardi, A.; Bloino, J.; Li, X.; Barone, V. Computational Simulation of Vibrationally Resolved Spectra for Spin-Forbidden Transitions. *Chirality* **2018**, *30*, 850–865.
(47) te Velde, G.; Bickelhaupt, F. M.; Baerends, E. J.; Fonseca Guerra, C.; van Gisbergen, S. J. A.; Snijders, J. G.; Ziegler, T. Chemistry with ADF. *J. Comput. Chem.* **2001,** *22*, 931.
(48) Lenthe, E. van; Baerends, E. J. Optimized Slater-Type Basis Sets for the Elements 1-118. *J. Comput. Chem.* **2003**, *24*, 1142–1156.
(49) Neese, F.; Wennmohs, F.; Becker, U.; Riplinger, C. The ORCA Quantum Chemistry Program Package. *J. Chem. Phys.* **2020**, *152*, 224108.
(50) Hirata, S.; Head–Gordon, M. Time–Dependent Density Functional Theory Within the Tamm–Dancoff Approximation. *Chem. Phys. Lett.* **1999**, *314*, 291–299.
(51) Peach, M. J. G.; Williamson, M. J.; Tozer, D. J. Influence of Triplet Instabilities in TDDFT. *J. Chem. Theory Comput.* **2011**, *7*, 3578–3585.
(52) Mayorga Burrezo, P.; Jiménez, V. G.; Blasi, D.; Ratera, I.; Campaña, A. G.; Veciana, J. Organic Free Radicals as Circularly Polarized Luminescence Emitters. *Angew. Chem. Int. Ed.* **2019**, *58*, 16282–16288.
(53) Zhang, D. -W.; Li, M.; Chen, C. -F. Linear Axially Chiral Conjugated Polymers Exhibiting Ultralong Low-Temperature Phosphorescence and Intense Circularly Polarized Luminescence. *Angew. Chem. Int. Ed.* **2022**, *61*, e2022131.